ADVANCED OPTICAL MATERIALS
www.advopticalmat.de

Highly Luminescent Organic Nanorods from Air Oxidation of *para*-Substituted Anilines for Freestanding Deep-Red Color Filters

*Yoonsang Park, Cheolwoo Park, Joo Sung Kim, Tae Kyu Ahn, Ho Sun Lim, Tae-Woo Lee, and Woosung Kwon**

Oxidation of aniline provides useful organic nanostructures with a wide variety of particle morphologies and properties. Accordingly, in the present study, novel luminescent organic nanorods (ONs) are synthesized through one-step air oxidation of *para*-substituted anilines without any shape-guiding surfactants. These ONs present highly crystalline rod-like structures due to the *ortho*-coupling reaction of aniline and π–π interactions between the phenazine-like structures. Using photoluminescence spectroscopy, absorption spectroscopy, time-correlated single photon counting, and time-dependent density functional theory calculation, it is revealed that the phenazine-like structures in the ONs are largely responsible for their bright, photostable, deep-red luminescence with absolute quantum efficiency up to 46%. Finally, the potential application of ONs as a freestanding color filter for deep-red-light-emitting devices that could be used for color pixels of future displays is demonstrated. The findings of this study provide a new strategy for the preparation of luminescent organic nanomaterials, and show their potential for optoelectronic applications.

1. Introduction

Over the past decade, numerous luminescent nanostructures including organic–inorganic hybrid nanostructures and inorganic semiconductors have been invented and investigated for various applications such as light-emitting diodes (OLEDs), solar cells, phosphors, and sensors.[1–4] On the other hand, studies for synthesizing luminescent organic nanostructures have been carried out only a few recent studies.[5] Yet, luminescent organic nanostructures have superior competitiveness compared to other nanostructures in terms of easy fabrication, flexibility, environmental stability, and low cost. Especially, luminescent 1D organic nanostructures based on organic π-conjugated molecules take rising attention as building blocks for several unique functional devices such as lasers, waveguides, solar cells, and field-effect transistors.[6,7] Although several success in constructing luminescent 1D organic materials by self-assembly or self-organization were achieved, the synthesis of those materials starts from preparing luminescent organic molecules, which are produced from over several organic reaction and purification steps, requiring significant time, skill, and attention. Therefore, the study of novel luminescent 1D organic nanostructures which can be synthesized directly from nonluminescent simple organic molecules has great advantages.

On the other hand, aniline is one of the most fundamental compounds available to the chemical industry and has been employed consistently and extensively since its discovery in 1826. Decades of research on the oxidation of aniline have revealed that controlling the reaction conditions, such as pH, solvent, and reaction temperature, as well as the judicious choice of oxidant, dopant (if any), and catalyst, can afford a variety of multidimensional organic nanostructures, including nanotubes, nanofibers, nanowires, and nanoplates,[8–16] and they have been applied in numerous useful products, such as dyes, explosives, and polymers.[17–23]

In the current study, we found that the air oxidation of particular *para*-substituted anilines in organic media yields highly crystalline 1D organic nanorods (ONs) composed of π–π stacked

Y. Park
Department of Chemical Engineering
Pohang University of Science and Technology (POSTECH)
77 Cheongam-ro, Nam-gu, Pohang, Gyeongsangbuk-do 37673
South Korea
C. Park, Prof. T. K. Ahn
Department of Energy Science
Sungkyunkwan University
2066 Seobu-ro, Jangan-gu, Suwon, Gyeonggi-do 16419, South Korea
J. S. Kim, Prof. T.-W. Lee
Department of Materials Science and Engineering
Institute of Engineering Research
Research Institute of Advanced Materials
BK21 PLUS SNU Materials Division for Educating Creative Global Leaders
Seoul National University
1 Gwanak-ro, Gwanak-gu, Seoul 08826, South Korea
Prof. H. S. Lim, Prof. W. Kwon
Department of Chemical and Biological Engineering
Sookmyung Women's University
100 Cheongpa-ro 47-gil, Seoul 04310, South Korea
E-mail: wkwon@sookmyung.ac.kr
The ORCID identification number(s) for the author(s) of this article can be found under https://doi.org/10.1002/adom.201800577.

DOI: 10.1002/adom.201800577

phenazine-like structures. Interestingly, these reactions are performed without using shape-guiding surfactants. Furthermore, the synthesized ONs show bright and stable red photoluminescence (PL) with high quantum yields (QYs) of up to 46% and reasonable full-width-at-half-maximum (FWHM) values (≈25 nm). To the best of the authors' knowledge, no research on producing luminescent 1D organic nanostructures from single anilines via single-step reactions has been conducted. We have proposed a plausible mechanism for the nanorod formation on the basis of structural/chemical and ab initio analyses. We have also investigated the origin of the red PL and how the *para*-substituents of the anilines affect the structures and optical properties of our ONs. Finally, we demonstrate the real-world utility of these ONs by fabricating red-light-emitting devices (r-LEDs) with ON-based color filters that produce high-quality deep-red luminescence.

2. Results and Discussion

2.1. Synthesis and Chemical Characterization

In general, the oxidation of aniline induces *ortho*- or *para*-coupling of aniline molecules via electrophilic substitution (**Figure 1**a).[9,24] The *para*-coupling of aniline molecules affords the conducting polymer polyaniline (PANI), while *ortho*-coupling of aniline produces planar sheet-like phenazine-like structures by intramolecular cyclization.[25,26] We used *p*-fluoroaniline (F-aniline), *p*-ethylaniline (C-aniline), *p*-(methylthio)aniline (S-aniline), and N-phenyl-*p*-phenylenediamine (N-aniline) to prepare four different types of ONs, labeled F-ON, C-ON, S-ON, and N-ON, respectively. The functional groups of these precursors were selected based on their heat and oxidation stabilities, which could be determined from the boiling points and *para*-position Hammett substituent constants of the precursors, respectively (Table SX, Supporting Information). The reactions were carried out in toluene to solubilize the anilines and avoid the effects of CO_2, which will be discussed later. Since the *para*-coupling reaction is prevented by *para*-substituents, air oxidation results in *ortho*-coupling alone, producing phenazine-like structures that form 1D nanorods (Figure 1b). The driving force of the nanorod formation seems to be a planar sheet-like orientation and π–π stacking of the phenazine-like structures, similar to the strategy of controlling the macroscopic shape of PANI-based materials.[24,27]

The rod-like structures of the ONs can be confirmed by reference to the transmission electron microscopy (TEM) images (**Figure 2**a–d and Figure S1, Supporting Information). The high-resolution TEM images in Figure 2e show the distinct crystalline phase in the ONs with a lattice spacing of 0.306 nm, which is a typical intermolecular distance for π–π stacked molecules,[28] indicating that the nanorods are composed of π–π stacked phenazine-like nanoplanes. The aspect ratio of the ONs is ≈7.5 regardless of *para*-substituents, which indicates that the formation of ONs is not affected by the *para*-substituent unless it is oxidized or removed (Figure 2f). The average width and length of the ONs are ≈6 nm and ≈45 nm, respectively (Figure S2, Supporting Information). The rod-like structures of ONs are also confirmed by atomic force microscopy (AFM) (Figure S3, Supporting Information). The height profiles in Figure S3c,d (Supporting Information) show the height of the ON is 7 nm, which is much smaller than the width (20 nm), indicating that the ON has asymmetric rod shape rather than a cylindrical shape. This appears to be due to the growth of rod-shape caused by π–π stacking of the plane-shaped phenazine-like structures.

To analyze the chemical structure of the ONs, X-ray photoelectron spectroscopy (XPS) was conducted. As shown

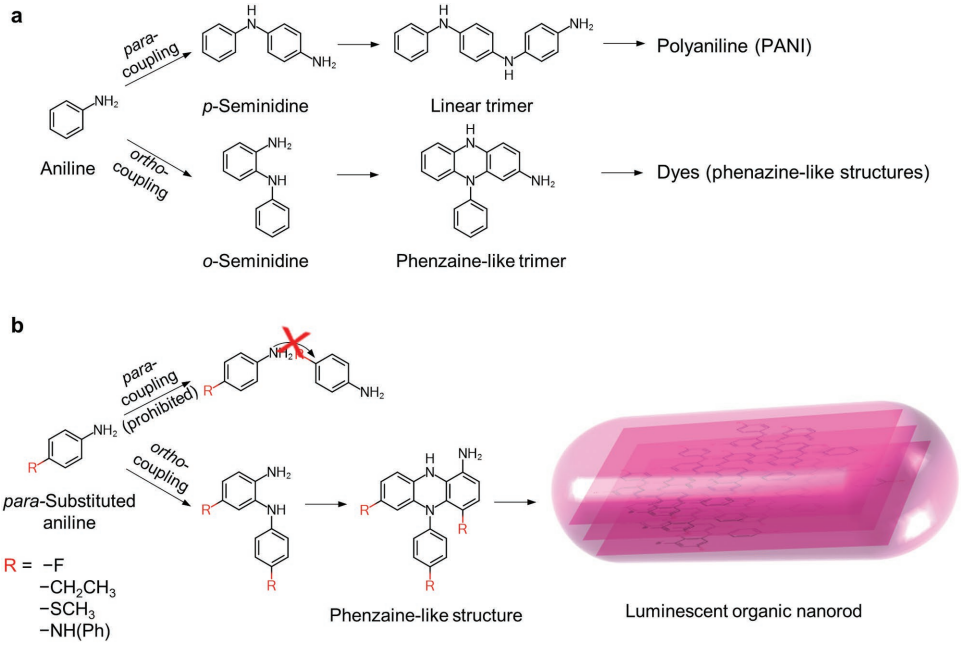

Figure 1. a) Oxidative coupling of aniline molecules. b) Proposed mechanism for the formation of ONs.

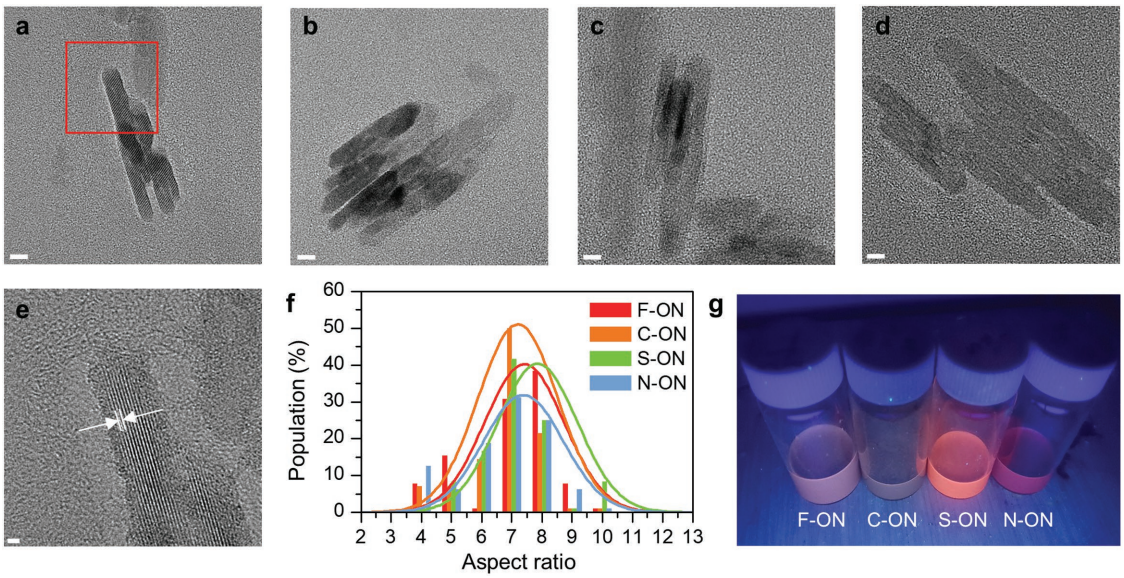

Figure 2. a–d) TEM images of F-ON, C-ON, S-ON, and N-ON. The scale bars represent 5 nm. e) High-resolution TEM image of ONs. The image is a magnification of the area highlighted by the red square in (a). The scale bar represents 1 nm. f) Aspect ratio distributions for F-, C-, S-, and N-ONs. Average values (avg.) and standard deviations (σ) for each type of ONs are represented as follows: avg. = 7.41/7.2/7.85/7.39, σ = 1.32/1.04/1.32/1.67 (from left to right, F-, C-, S-, and N-ONs). g) ONs under a 365 nm UV lamp.

in Figure S4 (Supporting Information), the deconvoluted C1s XPS spectra of all the ONs show the presence of C—C/C=C (284–285 eV) and C—N peaks (285.8–286.2 eV) due to the phenazine-like structures and anilines. The presence of the carbonyl C=O peak (287.8–288.0 eV) may be attributed to oxygen-containing defects (phenols, quinones, etc.) in the ONs formed upon air oxidation.[29–31] The absence of the carbonyl peak for S-ONs indicates that unobservable amount of carbonyl species develop during the air oxidation of S-ON. Conversely, the C-ONs present intense carbonyl peaks, which appear to be due to oxidation of the ethyl groups. The elemental analysis results in Table S1 (Supporting Information) show the F, C, S, and N contents of the ONs, indicating that the *para*-substituents are not removed during the oxidation process. In addition, all the ONs show non-negligible oxygen contents (7–24%), which appear to come from the aforementioned oxygen-containing defects resulting from air oxidation.

To confirm the presence of phenazine-like structures in the ONs, we performed Fourier-transform infrared (FTIR) and nuclear magnetic resonance (NMR) analyses. As shown in **Figure 3** and Figure S5a (Supporting Information), the FTIR spectra of the aniline precursors and the ONs all feature aromatic out-of-plane bending (825 cm^{-1}), aromatic in-plane C—H bending (1050–1200 cm^{-1}), aromatic C—C stretching (1495 cm^{-1}), and aromatic C—H stretching peaks (3000–3100 cm^{-1}), indicating that some aromatic structures from the aniline precursors remain in the ONs (green shade). In addition, the aniline N—H bond stretching band (3200–3500 cm^{-1}) is still observed for the ONs, even though most of the amino groups are removed during the nanorod formation. Thus, this band is attributed to the presence of terminal amino groups at the edges of the ON structures.

The FTIR spectra of the ONs show the development of several additional peaks when compared to those of the aniline precursors, indicating that more complex conjugated ring structures are formed in the ONs (Figure S5b, Supporting Information). Specifically, C—N stretching of the primary aromatic amine (1230 cm^{-1}),[32] skeletal C=C stretching of the *ortho*-linked aniline constitutional units (1445 cm^{-1}),[33] and stretching peaks for the phenazine-like structures (1080, 1357, 1445, 1550, and 1630–1750 cm^{-1})[9,11,33–35] indicate the presence of phenazine-like structures in the ONs. The alkyl C—H stretching peaks (2800–2950 cm^{-1}) are attributed to alkyl groups in the *para*-substituents and residual toluene. The peaks observed at ≈3243 cm^{-1} are assigned to hydrogen-bonded N—H···N stretching of the secondary amine, indicating the presence of intra- and intermolecular hydrogen bonds in the ONs.[27] The peaks at ≈3650 cm^{-1} are attributed to O—H stretching of hydroxyl groups, indicating the presence of oxygen-containing defects in the ONs, such as phenols and quinones, as discussed earlier.

The ^{1}H NMR spectra also present signals that indicate that phenazine-like structures are present in the ONs. The ONs present amine group hydrogen peaks at 3.5–4.0 ppm that are smaller than those observed for the corresponding precursors (Figure S6, Supporting Information), revealing that most of the amino group hydrogens are removed during the nanorod formation. In addition, the development of new aromatic signals at 7.08, 7.43, and 7.1–7.3 ppm for the ONs indicates that the aniline-ring structures are converted to more complex aromatic structures, such as phenazine-like structures.[36] The simulated spectra shown in Figure S7 (Supporting Information) confirm that phenazine-like structures present aromatic signals in the corresponding region. Conversely, the presence of alkyl groups in C- and S-aniline leads to alkyl peaks (2.4–2.8 ppm) in the ^{1}H NMR spectra of C-aniline, S-aniline, C-ON, and S-ON (Figure S6c–f, Supporting Information). Unlike their aniline precursors, which show single hydrogen peaks, C- and S-ONs

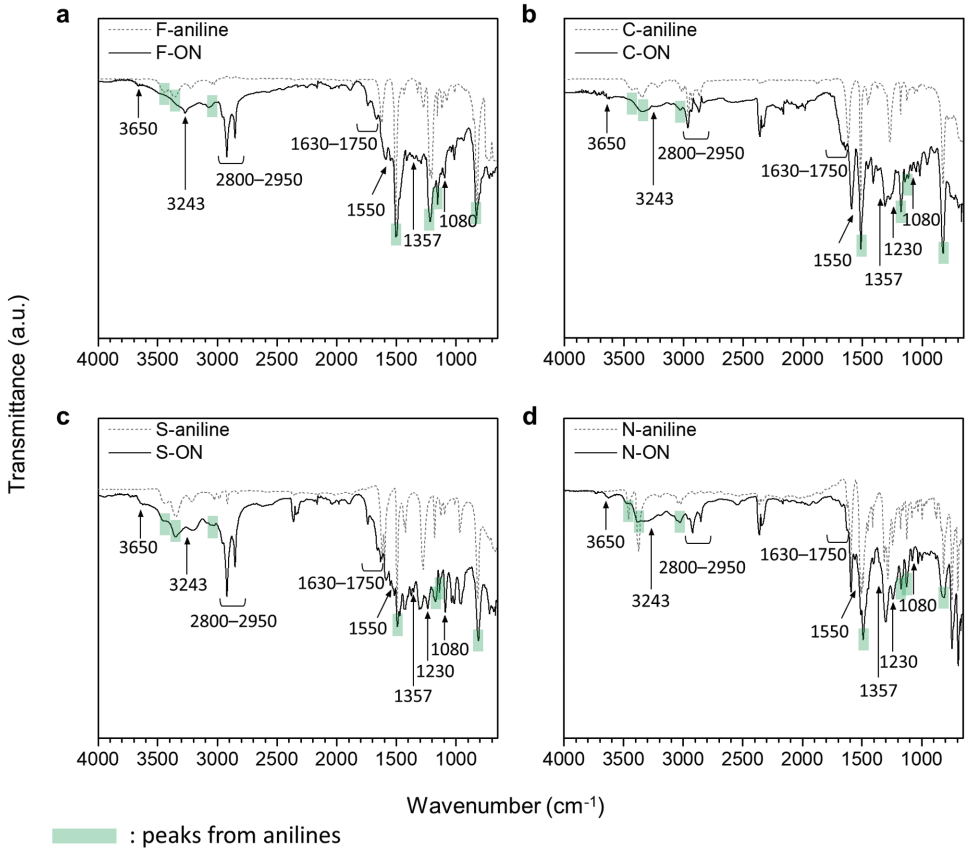

Figure 3. a–d) FTIR spectra of F-ON, C-ON, S-ON, and N-ON. Each spectrum is plotted together with that of its corresponding aniline precursor (upper curve, gray dotted lines).

present multiple alkyl signals, indicating that alkyl hydrogens in various chemical environments are present in the ONs. This further indicates that the *para*-substituted anilines are polymerized, forming complex structures such as phenazine-like species. Accordingly, the simulated spectrum in Figure S7b (Supporting Information) also shows multiple alkyl signals. Further details of all the chemical analyses are provided in the Supporting Information.

2.2. Optical Characterization and Electronic Structure

2.2.1. Optical Properties of ONs

Our ONs all show bright PL in the red region. Thus, in order to investigate these optical properties and the origin of the PL, we conducted UV–vis absorption spectroscopy and PL spectroscopy studies. A shown in Figure S8 (Supporting Information), the UV–vis spectra of the ONs show strong absorption bands in the 500–600 nm region. Similarly located absorption bands have been observed for phenazine dyes such as safranin and pseudo-mauveine,[26,27,37] suggesting that the absorption bands for the ONs originate from phenazine-like structures. Also, the gradual absorption curve in 200–500 nm region may indicate the existence of various energy states such as oxygen-containing defect states. To identify the PL-responsible absorptions, we plotted PL excitation maps (i.e., a set of excitation spectra) for each of the ONs (**Figure 4**a–d). The PL excitation maps show sharp and distinct excitation peaks at 575 (F-ON), 560 (C-ON), 585 (S-ON), and 600 (N-ON) nm, which correspond to the absorption bands for phenazine dyes. The excitation peak position shifts depending on the substituents in the ONs, which is presumably due to the bathochromic effect of the electron-donating groups of the *para*-substituents. The degree of these bathochromic shifts is inversely proportional to the electronegativity of the *para*-substituents, except that for the F-ON sample. The unexpected redshift for F-ON may be attributed to the high intrinsic polarity of the fluorine substituents.

The excitation characteristics of the ONs were also investigated by time-dependent density functional theory (TDDFT) analysis of phenazine-like structures using the B3LYP/6-311+ basis set (Figure 4e–h and Figure S9, Supporting Information). From the calculated molecular orbital configurations, we established that the first excited singlet state is $S_1(\pi,\pi^*)$ in all of the phenazine-like structures. According to Mataga and Ezumi, the first excited single state for some phenazine derivatives is $S_1(\pi,\pi^*)$, which allows for radiative recombination in these molecules.[37] In contrast, the first excited singlet state of the phenazine molecule is $S_1(n,\pi^*)$, meaning that it is nonfluorescent. Furthermore, the calculated excitation energies for the phenazine-like structures match the experimentally observed excitation energies well, indicating that the PL emissions

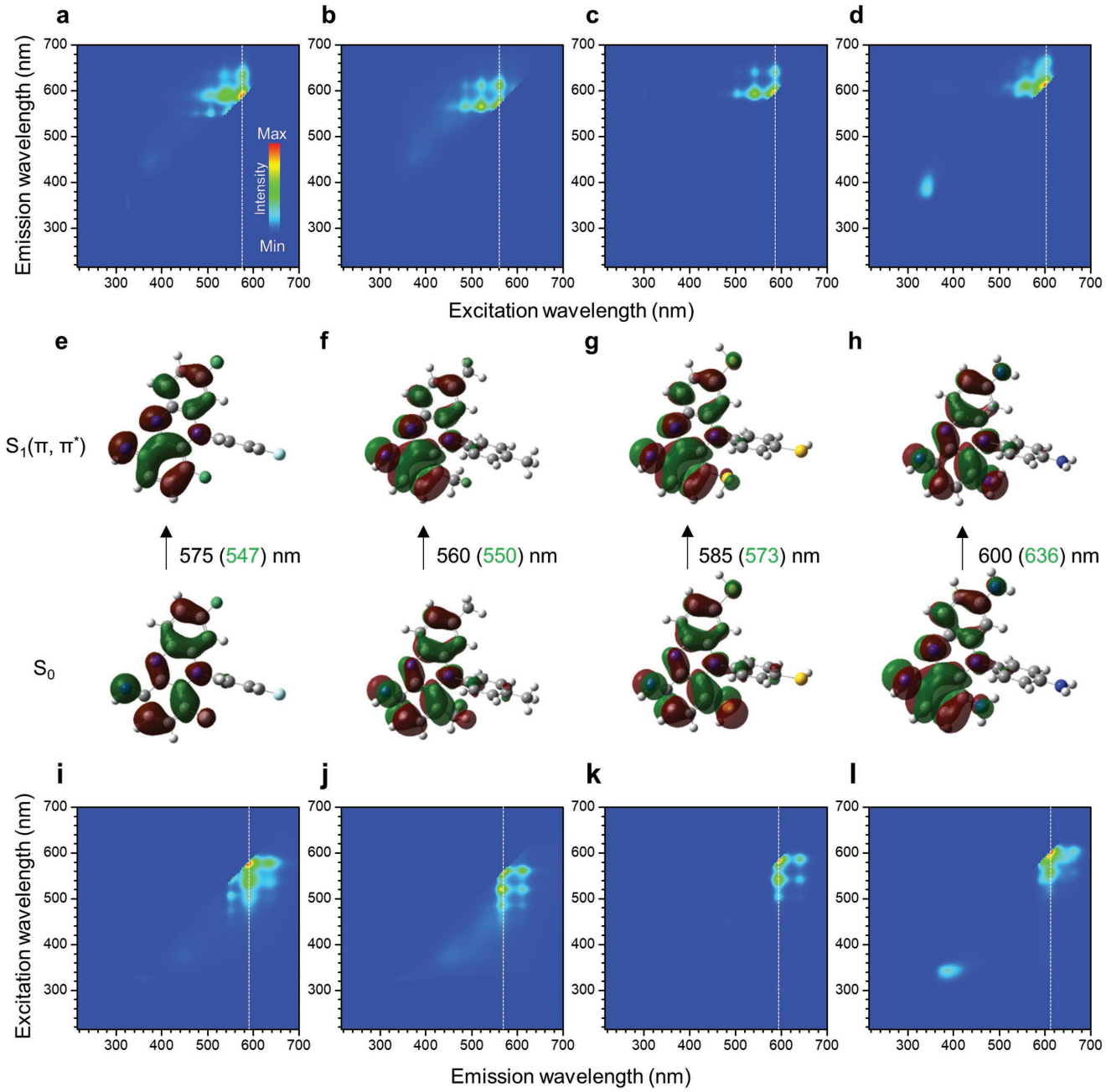

Figure 4. a–d) PL excitation maps and e–h) their corresponding energy level diagrams for F-ON (a,e), C-ON (b,f), S-ON (c,g), and N-ON (d,h). The ground and first excited states are denoted as S_0 and S_1. The experimental excitation wavelengths and simulated excitation wavelengths are shown in black and green, respectively. i–l) PL emission maps of F-ON, C-ON, S-ON, and N-ON.

originate from radiative transition from the first excited singlet state ($S_1(\pi,\pi^*)$) to the ground state (S_0) of the phenazine-like structures in the ONs. Since our calculations did not account for solvation characteristics, the TDDFT calculation results for F-ON show a certain degree of deviation (equivalent to 10–20 nm or ≈0.1 eV) from the experimental results. More details on the calculation analyses are provided in the Supporting Information.

The PL emission maps (i.e., a set of emission spectra) for the ONs in Figure 4i–l show sharp and narrow emission peaks at 590 (F-ON), 575 (C-ON), 595 (S-ON), and 610 (N-ON) nm. The FWHM values for the ONs are ≈25 nm, which is comparable to those of semiconductor quantum dots (30–40 nm). The minor peaks detected at longer wavelengths (≈30 nm) are attributed to the vibronic transitions of highest occupied molecular orbital (HOMO) and lowest unoccupied molecular orbital (LUMO) states, which are typically observed in organic fluorophores.[38] Furthermore, for the F-, C-, and N-ON samples, relatively small emission bands appear in the 400–500 nm region, presumably due to oxygen-containing defects.

2.2.2. Electronic Structures of ONs

To investigate the energy structures of the ONs, time-correlated single photon counting (TCSPC) analysis was conducted. As shown in Figure S10 (Supporting Information), the TCSPC signals for F-ON, S-ON, and N-ON, which were recorded at their respective PL peaks under an excitation wavelength of 485 nm, are fitted by a single-exponential decay model, and their lifetime (τ) components are almost the same, that is, ≈2.5–3.5 ns (Table S3, Supporting Information). This implies that a common specific emissive state or energy structure exists in our ONs, presumably originating from the phenazine-like structures. It is noteworthy that the C-ONs show two distinct lifetime components in their decay signal, a shorter one (0.70 ns) and a longer one (3.48 ns), implying that at least two radiative recombination pathways exist for this material. The shorter lifetime might be due to rapid recombination that takes place in the oxygen-containing defects,[39] as the C-ONs contain more carbonyl moieties than the other ONs, as demonstrated by the XPS data. The longer lifetime has the same order of magnitude as those of the other ONs, so we can postulate that this recombination pathway is related to the phenazine-like structures.

On the other hand, the absolute quantum yields (QYs) were also measured for the ONs (Figure S11, Supporting Information). The QYs are 3.7, 0.5, 27.2, and 7.7% for F-, C-, S-, and N-ONs, respectively. Even though the average lifetime values for the ONs are similar, significant differences are observed in their QYs. This is because many nonradiative energy states related to chemical and structural defects exist in the ONs and absorb photons (Figure S8, Supporting Information). The XPS results shown in Figure S4 (Supporting Information) indicate that the QYs are inversely proportional to the amount of carbonyl moieties in the ONs. Thus, the highest QY is observed for the S-ONs, which has the lowest oxygen content according to XPS and elemental analysis. Also, for S-ONs, the removal of highly oxidized (i.e., high-polarity) ONs from slightly oxidized (i.e., low-polarity) ONs using 1-octadecene (i.e., a nonpolar solvent) increases the QY to 46% (Figure S12, Supporting Information), which is consistent with the previous results.

Accordingly, it can be concluded that there are two types of emissive states in the ONs: a major state from the phenazine-like structures and a defective state from the oxygen-containing defects, as depicted in Figure S13 (Supporting Information). We reasoned that the emissive states associated with the phenazine-like structures could be one of the origins of the red PL observed for several organic and carbonaceous nanostructures (e.g., carbon nanodots) prepared using *para*-substituted anilines (e.g., *para*-phenylenediamine) as a precursor.[40–43]

2.2.3. Photostability of ONs

To test the stability of the ONs, photostability and long-term stability tests were conducted. As shown in Figure S14 (Supporting Information), the ONs show superior photostabilities to those of organic fluorophores such as resorufin. Upon exposure to 365 nm UV light (6 W), the PL of resorufin decreases to 15% of its initial value after 2 h and virtually disappears after 6 h. In contrast, the PLs of the ONs are largely conserved (>80%) under the same conditions. Furthermore, as shown in Figure S15 (Supporting Information), the S-ONs show almost no change in PL emission over more than three months under ambient conditions. Thus, the ONs exhibit the long-term stabilities required for practical application.

2.3. Effects of Reaction Conditions

2.3.1. Effects of Atmospheric Conditions

Because the presence of phenazine-like structures in ONs can be confirmed by PL analysis, we assessed the PL of the products from the air oxidation of various substituted aniline precursors prepared under different reaction conditions in order to investigate the ON formation process more precisely. First, to confirm that oxidation in air is crucial for nanorod formation, we attempted an S-ON synthesis under argon instead of air. The product showed none of the PL characteristics observed for S-ONs, indicating that nanorod formation occurs by air oxidation (Figure S16, Supporting Information).

2.3.2. Effects of Reaction Time

To explore the effect of reaction time, the time was varied from 4 to 24 h. As the reaction time increases, the color of the product turns dark-red to rose-red and the PL of the sample is increased (Figure S17, Supporting Information). Also, by increasing reaction time, the FTIR spectra show the decrease of original aniline peaks at 1275, 1421, 1493 (ring in-plane stretching), and 1597–1618 cm^{-1} (N—H—H angle widening), development of the stretching peaks of phenazine-like structures at 1080, 1357, 1445, and 1550 cm^{-1}, and increase of sp^2 C—H stretching at 2800–2950 cm^{-1}, indicating that the aniline structures turns into phenazine-like structures (Figure S18, Supporting Information). The TEM images show that the rod-like morphologies are grown up by increasing reaction time (Figure S19, Supporting Information). Combining these results, it is concluded that the nanorod growth is directly related with the formation of phenazine-like structures.

2.3.3. Effects of Substituent Groups of Aniline

In addition, to investigate the effect of the aniline substituent position, we attempted to prepare nanorods with nonsubstituted aniline, 2,4,6-substituted aniline, and 2,3,4-substituted aniline (Figure S20a–c, Supporting Information). According to our hypothesis, *para*-substituents induce *ortho*-coupling of anilines. Thus, if the *para*-position is not substituted (nonsubstituted aniline) or the *ortho*-position is substituted (2,4,6-substituted aniline), the formation of phenazine-like structures will not occur. In line with our predictions, the air oxidation products of nonsubstituted aniline and 2,4,6-substituted aniline do not show red PL, and only the 2,3,4-substituted aniline product exhibits strong red PL (Figure S20d–f, Supporting Information). The broadened PL bandwidth is due to the increased polarity of the ONs owing to the large number of fluorine substituents.

Substituent stability is also important because, if the substituents are easily oxidized or released during oxidation, nanorod formation will be interrupted. We subjected *para*-position ester-substituted aniline (ethyl-4-aminobenzoate) to air oxidation. Consequently, the ester group was oxidized to a carboxylic group, and polymeric structures were synthesized instead of nanorods (Figure S21, Supporting Information). Furthermore, the PL maps show green PL centered at 490 nm instead of the red PL observed for the phenazine-like structures.

2.3.4. Effects of Solvent Polarity

Nanorod formation is also highly dependent on solvent polarity. When the synthesis of nanorods is performed in a polar solvent such as anisole and dimethyl sulfoxide (DMSO), they emit at a blue-to-green wavelength near 450 nm (Figure S22a,b, Supporting Information). The relative intensity of the blue-to-green emission peak to the red-emission peak of ON is higher when DMSO was used as a solvent than the anisole, which means that this blue-to-green emission is related to the polarity of the solvent (relative polarity of anisole = 0.198, DMSO = 0.444). Also, the FTIR spectrum of the product using DMSO as solvent shows a strong broad peak at 3100–3400 cm^{-1} and strong sharp peak at 1630 cm^{-1}, which are characteristic peaks of the amide compound and no such peaks were observed in ONs (Figure S22d, Supporting Information). Also, the TEM images of the product indicate that the nanorod was not successfully formed in DMSO solvent and the blue-to-green emission is originated from side reactions (Figure S22e, Supporting Information).

As the solubility of CO_2 and water increase with increasing solvent polarity, the side reaction in which aniline reacts with CO_2 to yield anilide seems to occur mainly in polar solvents (Figure S23a, Supporting Information). This hypothesis can explain the amide peak observed in the FTIR spectrum. The hypothesis is also supported by the fact that a variety of substituted-aniline molecules emit light in the same blue-to-green wavelength region following reaction with carboxyl species such as acetic acid to yield anilide species (Figure S23b–d, Supporting Information). The blue-to-green emission seems to originate from a radiative transition from $S_1(n,\pi^*)$ to S_0 in anilide species resulting from the reaction of aniline and CO_2.[44,45]

2.3.5. Effects of Reaction Temperature

The reaction temperature is also critical in air oxidation. As shown in Figure S24 (Supporting Information), at high temperature (>250 °C), the product showed blue emission bands at 380–420 nm, presumably due to the formation of anilide species or carbonization of aniline. In high temperature and oxidative condition, many organic molecules tend to carbonize to form carbonized nanoparticles.[46–50] Carbonized particles generally exhibit dark color and long-range absorption due to the formation of various energy states from carbonization. Also, the blue luminescence from the carbonized nanoparticle is very common phenomenon.[46–48] The sample synthesized at high temperature clearly showed long-range absorption in the 200–800 nm range (Figure S24c, Supporting Information) and dark-gray color (Figure S24d, Supporting Information), indicating that carbonization process occurred during the synthesis.

2.4. Fabrication of Freestanding Deep-Red Color Filters

Finally, we fabricated r-LEDs using our ONs as a freestanding color filter. We chose S-ONs to prepare the r-LEDs since they exhibit the superior PL, QY, and photostability to other ONs. The color filters were fabricated by drop casting the mixed solution of S-ONs and poly(methyl methacrylate) (PMMA). In the color filters, S-ONs were uniformly dispersed and embedded in a transparent PMMA matrix and showed almost uniform PL spectra regardless of the locations of the filter (Figure S25, Supporting Information). By positioning the color filters over white-LEDs and applying a forward-bias current of 50 mA (≈4 V, optimized), we obtained deep-red light with the peak wavelength λ_{max} = 680 nm, as shown in **Figure 5**a,b. Furthermore, as shown in Figure 5c,d, the device exhibits the Commission Internationale d'Eclairage (CIE) coordinates (0.7197, 0.2783), which are similar to the chromaticity of the red primary colors of the Adobe RGB color space (0.64, 0.33). Thus, owing to their flexibility and high color purity, the ON-based color filters could be used for color pixels of future displays.

3. Conclusion

We synthesized luminescent ONs via template-free air oxidation of *para*-substituted anilines (F-, C-, S-, and N-anilines) in toluene. The obtained F-, C-, S-, and N-ONs show highly crystalline 1D nanorod structures. It is proposed that the driving force of the nanorod formation is the growth of phenazine-like structures due to the *ortho*-coupling of *para*-substituted anilines. The ONs are composed of π–π stacked phenazine-like structures, which are concluded to be responsible for the PL on the basis of optical and ab initio analyses. The ONs show bright red PL with high QYs (up to 46%), small FWHM (≈25 nm), and high photostability. The ONs were applied as a freestanding color filter in an r-LED, successfully producing bright deep-red light. Thus, our ONs prepared by one-step template-free synthesis exhibit excellent optical properties, making them highly attractive for various optoelectronic applications.

4. Experimental Section

Synthesis of Luminescent ONs: 4-Fluoroaniline (5 mmol) was dissolved in toluene (5 mL) and the solution was heated for 36 h at 85 °C with vigorous stirring in air. To prevent complete solvent evaporation during the reaction, extra toluene (5 mL) was added every 12 h. After cooling to room temperature, the sticky liquid remaining was dissolved in toluene (5 mL) and then dialyzed against toluene for at least 72 h using Spectra/Por Biotech Cellulose Ester dialysis tubes (100–500 Da). The solution was evaporated to dryness on a rotary evaporator to yield F-ONs. C-ONs, S-ONs, and N-ONs were prepared by the same method, but with 4-ethylaniline, 4-(methylthio)aniline, and 4-aminodiphenylamine, respectively, being used instead of 4-fluoroaniline.

Characterizations: TEM was performed using a JEOL JEM-2200FS equipped with a Cs corrector. AFM was performed using a Park Systems

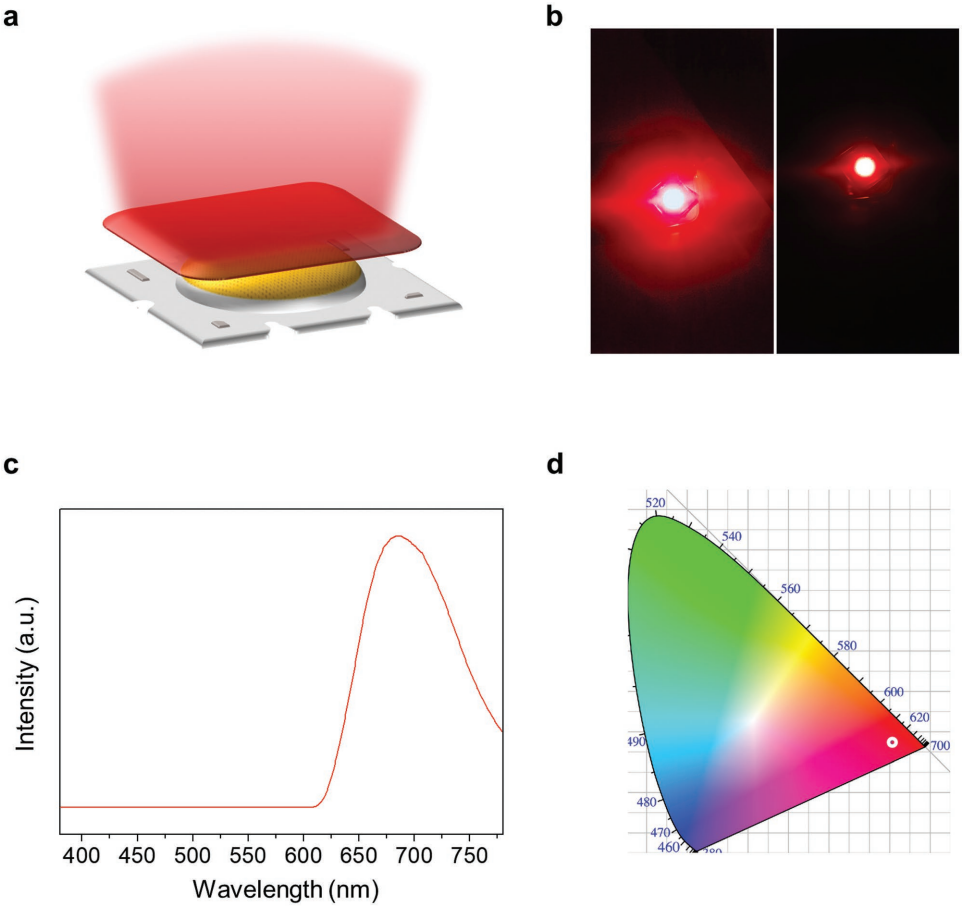

Figure 5. a) Illustration of r-LEDs employing S-ONs. b) Photographs of r-LEDs under operation. c) PL spectrum of r-LEDs. d) CIE chromaticity coordinates calculated from the PL spectrum.

NX-10. XPS was performed using an Escalab 250 spectrometer with an Al X-ray source (1486.6 eV). ^{1}H NMR spectra of the ONs dissolved in $CDCl_3$ were recorded on a Bruker DRX600 spectrometer (600 MHz). FTIR spectra were recorded on a Nicolet iS50 FTIR spectrometer. UV–vis absorption and PL spectroscopy was performed using 10 mm × 10 mm QS-grade quartz cuvettes (Hellma Analytics 111-QS). The light absorption spectra were recorded on a Scinco S-3100 spectrophotometer, and the PL spectra were recorded on a Jasco FP-8500 fluorometer. The quantum yields were measured using 2 mm × 10 mm QS-grade quartz cuvettes (Jasco Parts Center 6808-H250A). The absolute quantum yield data were obtained using a Jasco FP-8500 fluorometer equipped with a 100 mm integrating sphere setup (ILF-835) and analyzed using the Jasco Spectra Manager II software package. TCSPC measurements were performed using a FluoTim 200 TCSPC system (PicoQuant) with a variable repetition rate (0.8 MHz). The emitted TCSPC signal was spectrally dispersed by a monochromator (ScienceTech 9030) and was collected by a fast photon multiplier tube (PMT) detector (PMA 182, PicoQuant-GmbH). For the UV–vis, PL, and TCSPC analyses, the sample solutions were prepared in toluene. For computational analysis, all the calculations were performed using the Gaussian 09 suite of codes on a standard personal computer. For visualization, the GaussView 5.0 molecular visualization program was used. The DFT calculations and TDDFT calculations were performed using the B3LYP/6-311+ basis set.

Demonstration of r-LEDs: To fabricate color-converting films, S-ONs were dissolved in toluene (40 mg mL^{-1}). A 5 mL aliquot of the solution was mixed with 5 mL of a 10 wt% anisole solution of poly(methyl methacrylate). The mixture was vortexed for 10 min and then the air bubbles were removed. An aliquot of the mixture was drop-cast on a cleaned glass substrate (1 mL per 10 cm^2). The coated glass substrate was left overnight on a flat table under ambient conditions to allow the solvent to evaporate. The resulting films were peeled from the substrate and placed over white-light-emitting diodes (FH341B, Samsung) using adhesive tape to fabricate the r-LEDs. The PL spectra of the r-LEDs were measured using a computer-controlled source-measurement unit (Keithley 236) and a Minolta CS2000 spectroradiometer.

Supporting Information

Supporting Information is available from the Wiley Online Library or from the author.

Acknowledgements

This work was supported by the Ministry of Science and ICT of Korea under the KIST Institutional Program (2E28200-18-018), the Basic Science Research Program (NRF-2016R1C1B1011830), and partially the Nano Material Technology Development Program (2009-0082580). W.K. acknowledges Sookmyung Women's University Research Grant (1-1703-2005). The authors thank Sung In Kim (KANC) for her assistance with TEM. The authors also thank RIAM (Research Institute of Advanced Materials) for assistance with AFM.

Conflict of Interest

The authors declare no conflict of interest.

Keywords

aniline, luminescence, nanorods, phenazine, red emission

Received: April 30, 2018
Revised: July 2, 2018
Published online: September 5, 2018

[1] F. Wang, W. B. Tan, Y. Zhang, X. Fan, M. Wang, *Nanotechnology* **2006**, *17*, R1.
[2] J. Li, S. Guo, E. Wang, *RSC Adv.* **2012**, *2*, 3579.
[3] Y. Min, J. Li, F. Liu, P. Padmanabhan, E. K. L. Yeow, B. Xing, *Nanomaterials* **2014**, *4*, 129.
[4] A. Noy, A. E. Miller, J. E. Klare, B. L. Weeks, B. W. Woods, J. J. DeYoreo, *Nano Lett.* **2002**, *2*, 109.
[5] S. Li, L. He, F. Xiong, Y. Li, G. Yang, *J. Phys. Chem. B* **2004**, *108*, 10887.
[6] Y. Yan, C. Zhang, J. Yao, Y. S. Zhao, *Adv. Mater.* **2013**, *25*, 3627.
[7] X. Liu, D. Xu, R. Lu, B. Li, C. Qian, P. Xue, X. Zhang, H. Zhou, *Chem. Eur. J.* **2011**, *17*, 1660.
[8] H. D. Tran, J. M. D'Arcy, Y. Wang, P. J. Beltramo, V. A. Strong, R. B. Kaner, *J. Mater. Chem.* **2011**, *21*, 3534.
[9] J. Li, Q. Jia, J. Zhu, M. Zheng, *Polym. Int.* **2008**, *57*, 337.
[10] G. C. Li, Z. K. Zhang, *Macromolecules* **2004**, *37*, 2683.
[11] L. Zhang, L. Zhang, M. X. Wan, Y. Wei, *Synth. Met.* **2006**, *156*, 454.
[12] K. Huang, M. X. Wan, *Chem. Mater.* **2002**, *14*, 3486.
[13] X. Zhang, S. K. Manohar, *Chem. Commun.* **2004**, 2360.
[14] Y.-W. Cheng, L. Chao, Y.-M. Wang, K.-S. Ho, S.-Y. Shen, T.-H. Hsieh, Y.-Z. Wang, *Synth. Met.* **2013**, *168*, 48.
[15] C. Laslau, Z. D. Zujovic, L. Zhang, G. A. Bowmaker, J. Travas-Sejdic, *Chem. Mater.* **2009**, *21*, 954.
[16] X.-S. Du, C.-F. Zhou, G.-T. Wang, Y.-W. Mai, *Chem. Mater.* **2008**, *20*, 3806.
[17] I. Y. Sapurina, J. Stejskal, *Russ. J. Gen. Chem.* **2012**, *82*, 261.
[18] J. Stejskal, I. Sapurina, M. Trchová, E. N. Konyushenko, *Macromolecules* **2008**, *41*, 3530.
[19] I. Sapurina, J. Stejskal, *Polym. Int.* **2008**, *57*, 1295.
[20] Z. D. Zujovic, L. Zhang, G. A. Bowmaker, P. A. Kilmartin, J. Travas-Sejdic, *Macromolecules* **2008**, *41*, 3125.
[21] C.-G. Wu, D. C. DeGroot, H. O. Marcy, J. L. Schindler, C. R. Kannewurf, Y.-J. Liu, W. Hirpo, M. G. Kanatzidis, *Chem. Mater.* **1996**, *8*, 1992.
[22] E. M. Moujahid, M. Dubois, J.-P. Besse, F. Leroux, *Chem. Mater.* **2002**, *14*, 3799.
[23] J. M. Kinyanjui, D. W. Hatchett, *Chem. Mater.* **2004**, *16*, 3390.
[24] J. Stejskal, I. Sapurina, M. Trchová, *Prog. Polym. Sci.* **2010**, *35*, 1420.
[25] J. Stejskal, I. Sapurina, M. Trchová, E. N. Konyushenko, P. Holler, *Polymer* **2006**, *47*, 8253.
[26] J. Stejskal, M. Trchová, *Polym. Int.* **2012**, *61*, 240.
[27] Z. D. Zujovic, C. Laslau, G. A. Bowmaker, P. A. Kilmartin, A. L. Webber, S. P. Brown, J. Travas-Sejdic, *Macromolecules* **2010**, *43*, 662.
[28] C. Janiak, *J. Chem. Soc., Dalton Trans.* **2000**, 3885.
[29] A. Rakić, D. Bajuk-Bogdanović, M. Mojović, G. Ćirić-Marjanović, M. Milojević-Rakić, S. Mentus, B. Marjanović, M. Trchová, J. Stejskal, *Mater. Chem. Phys.* **2011**, *127*, 501.
[30] B. Marjanović, I. Juranić, G. Ćirić-Marjanović, *J. Phys. Chem. A* **2011**, *115*, 3536.
[31] E. J. Behrman, *J. Phys. Chem. A* **2011**, *115*, 7863.
[32] E. T. Kang, K. G. Neoh, K. L. Tan, *Prog. Polym. Sci.* **1998**, *23*, 277.
[33] M. Trchová, I. Šeděnková, E. N. Konyushenko, J. Stejskal, P. Holler, G. Ćirić-Marjanović, *J. Phys. Chem. B* **2006***110*, 9461.
[34] X.-S. Du, C.-F. Zhou, Y.-W. Mai, *J. Phys. Chem. C* **2008**, *112*, 19836.
[35] M. Trchová, J. Stejskal, *Pure Appl. Chem.* **2011**, *83*, 1803.
[36] J. Kříž, E. N. Konyushenko, M. Trchová, J. Stejskal, *Polym. Int.* **2011**, *60*, 1296.
[37] N. Mataga, K. Ezumi, *Bull. Chem. Soc. Jpn.* **1967**, *40*, 1350.
[38] Y. Honmou, S. Hirata, H. Komiyama, J. Hiyoshi, S. Kawauchi, T. Iyoda, M. Vacha, *Nat. Commun.* **2014**, *5*, 4666.
[39] M. Edge, N. S. Allen, R. Wiles, W. McDonald, S. V. Mortlock, *Polymer* **1995**, *36*, 227.
[40] K. Jiang, S. Sun, L. Zhang, Y. Lu, A. Wu, C. Cai, H. Lin, *Angew. Chem., Int. Ed.* **2015**, *54*, 5360.
[41] W. Kwon, S. Do, J.-H. Kim, M. S. Jeong, S.-W. Rhee, *Sci. Rep.* **2015**, *5*, 12604.
[42] H. Ding, S.-B. Yu, J.-S. Wei, H.-M. Xiong, *ACS Nano* **2016**, *10*, 484.
[43] A. M. Craciun, A. Diac, M. Focsan, C. Socacib, K. Magyari, D. Maniu, I. Mihalache, L. M. Veca, S. Astilean, A. Terec, *RSC Adv.* **2016**, *6*, 56944.
[44] I. Azumaya, H. Kagechika, Y. Fujiwara, M. Itoh, K. Yamaguchi, K. Shudo, *J. Am. Chem. Soc.* **1991**, *113*, 2833.
[45] P. Munshi, D. J. Heldebrant, E. P. McKoon, P. A. Kelly, C.-C. Tai, P. G. Jessop, *Tetrahedron Lett.* **2003**, *44*, 2725.
[46] X. Yan, X. Cui, B. Li, L.-S. Li, *Nano Lett.* **2010**, *10*, 1869.
[47] R. Liu, D. Wu, X. Feng, K. Müllen, *J. Am. Chem. Soc.* **2011**, *133*, 15221.
[48] P.-C. Hsu, H.-T. Chang, *Chem. Commun.* **2012**, *48*, 3984.
[49] A. B. Bourlinos, A. Stassinopoulos, D. Anglos, R. Zboril, V. Georgakilas, E. P. Giannelis, *Chem. Mater.* **2008**, *20*, 4539.
[50] A. B. Bourlinos, A. Stassinopoulos, D. Anglos, R. Zboril, M. Karakassides, E. P. Giannelis, *Small* **2008**, *4*, 455.